JGR Space Physics

RESEARCH ARTICLE
10.1029/2021JA029998

Mesospheric Nitric Oxide Transport in WACCM

Christine Smith-Johnsen[1], Daniel Robert Marsh[2,3], Anne K. Smith[2], Hilde Nesse Tyssøy[1], and Ville Maliniemi[1]

[1]Department of Physics and Technology, Birkeland Centre for Space Science, University of Bergen, Bergen, Norway, [2]National Center for Atmospheric Research, Boulder, CO, USA, [3]Faculty of Engineering and Physical Sciences, University of Leeds, Leeds, UK

Key Points:

- Whole Atmosphere Community Climate Model underestimates the mesospheric nitric oxide amount and the temperature profile is vertically displaced compared to SOFIE and SABER observations
- Changing the non-orographic gravity wave amplitude or Prandtl number modify where and how the modeled gravity wave energy and momentum are deposited
- Reducing the gravity wave amplitude improves both the vertical displacement of the summer mesopause and the wintertime mesospheric nitric oxide level

Correspondence to:
C. Smith-Johnsen,
christine.smith.johnsen@gmail.com

Citation:
Smith-Johnsen, C., Marsh, D. R., Smith, A. K., Tyssøy, H. N., & Maliniemi, V. (2022). Mesospheric nitric oxide transport in WACCM. *Journal of Geophysical Research: Space Physics*, *127*, e2021JA029998. https://doi.org/10.1029/2021JA029998

Received 27 SEP 2021
Accepted 18 FEB 2022

Abstract

Energetic particle precipitation (EPP) causes ionization of the main constituents of the Earth's atmosphere which leads to the production of nitric oxide (NO) throughout the polar mesosphere and lower thermosphere (MLT). Due to the long lifetime of NO during winter, it can also be transported deeper into the atmosphere by the mesospheric residual circulation (the indirect EEP effect). This study investigates the mesospheric indirect NO response to EEP using Whole Atmosphere Community Climate Model (WACCM) version 6. In comparison to observations from the instrument Solar Occultation For Ice Experiment (SOFIE) on the AIM (Aeronomy of Ice in the Mesosphere) satellite, a wintertime underestimation is found in the modeled mesospheric NO amount. WACCM's temperature profile is found to be vertically shifted compared to observations by SOFIE and by The Sounding of the Atmosphere using Broadband Emission Radiometry instrument on the Thermosphere Ionosphere Mesosphere Energetics Dynamics satellite (SABER). The discrepancies in NO are therefore attributed to the model's ability to simulate the dynamics responsible for the indirect EEP effect. The drivers of this transport are investigated by sensitivity runs of WACCM's gravity wave forcing. Changing the amplitude of the non-orographic gravity waves and the Prandtl number improves the modeled vertical distribution of NO and temperature in the MLT region.

Plain Language Summary

Nitric oxide (NO) is produced by energetic particle precipitation in the polar regions of the mesosphere and lower thermosphere, and its distribution rapidly increases with altitude. During winter the lifetime of NO is long enough for it to be transported by the downward atmospheric circulation in the mesosphere far from where it was produced. This makes the level of NO in the mesosphere dependent on both the local production and on transport processes. When comparing simulated NO in the model Whole Atmosphere Community Climate Model (WACCM) to observations by the satellite instrument Solar Occultation For Ice Experiment, too little NO is found in the mesosphere even when the mesospheric production is accounted for in the model. This may be related to model errors in the transport from the thermosphere. Comparing model temperatures to those observed by two different satellite instruments confirms that there are some dynamic deficiencies. The mesospheric circulation is driven by breaking gravity waves, so by changing where and how the wave energy and momentum are deposited in WACCM, the modeled circulation can be altered to improve the vertical NO distribution and the temperature profile in the polar mesosphere and lower thermosphere. The best correspondence between modeled and observed nitric oxide and temperature is found when the amplitude of the gravity waves is reduced or when the eddy diffusion is increased.

1. Introduction

The main source of nitric oxides (NO) in the polar mesosphere and lower thermosphere (MLT) is the production by energetic electron precipitation (EEP; Gérard et al. [1984]). These are magnetospheric electrons that reach the Earth's atmosphere by spiraling along the geomagnetic field lines. Auroral electrons (1–30 keV) originate from the plasma sheet and can reach the thermosphere, while electrons accelerated to higher energies (30–1,000 keV) in the Earth's radiation belts can deposit their energy deep into the mesosphere. These energetic electrons will ionize the atmosphere which leads to the production of NO (called the direct EEP effect; Randall et al., 2006). The direct influence of particle precipitation on the MLT region has been studied since the 1970s (Barth et al., 2003; Cravens et al., 1985; Crutzen et al., 1975; Nicolet, 1975; Saetre et al., 2004; Swider et al., 1978; Weeks et al., 1972), but has only recently been included in the major reports studying change in climate (Eyring et al., 2016; IPCC, 2013; Matthes et al., 2017). NO has a lifetime of about 1 day under sunlit conditions, but in

the dark polar winter where no sunlight is present, NO can have an effective lifetime of months. The winter polar vortex constrains the NO to high latitudes where the residual atmospheric circulation is downward and transports it down toward the stratosphere (the indirect EEP effect; Randall et al., 2007). There, NO can catalytically destroy ozone (O_3), which is an important species for the atmosphere's radiative balance as it absorbs short-wave solar radiation and emits long-wave radiation. Changes in the O_3 abundance impact both temperature and dynamics. Perturbations of the NO content of the atmosphere can therefore have a significant impact on the O_3 composition (Crutzen, 1979; Jackman et al., 2008), subsequently, affect wave propagation and potentially provides a mechanism by which EEP effects can propagate down to impact the surface of the Earth (Arsenovic et al., 2016; Maliniemi et al., 2019; Seppälä et al., 2014).

The transport processes in the MLT responsible for the indirect EEP effect are advection, molecular diffusion, and eddy diffusion. In the polar mesosphere during winter, the downward transport is dominated by the residual circulation (Smith et al., 2011), which is driven by the breaking of gravity waves (Brasseur & Solomon, 2005). Molecular diffusion is caused by molecular movement and gravity and is especially important above the mesopause due to increased path length at low densities. The impact of molecular diffusion rapidly decreases with decreasing heights, while the impact of advection increases with decreasing heights. Eddy diffusion is transported by turbulent mixing and dissipating waves, and its main source in the mesosphere and the lower thermosphere is the breaking of gravity waves. Both eddy and molecular diffusion can transport high concentrations of thermospheric NO molecules downward across the mesopause, and when the NO reaches the mesosphere the residual circulation will take over and continue the downward transport. Molecular diffusion is insignificant compared to eddy diffusion below 100 km (Smith et al., 2011).

Where these processes dominate are determined by where the gravity waves break and how their energy and momentum are distributed. Gravity waves (GWs) are created in the troposphere by surface topography (orographic GWs) or by frontal systems and convection (non-orographic GWs). When GWs propagate upward vertically they encounter exponentially thinner air and due to the conservation of kinetic energy, the wave amplitude will grow exponentially with height (Eliassen & Palm, 1961). When the GW amplitude becomes too large to be convectively stable the GW break and deposit some of its energy. The breaking altitude is determined by the wave's starting amplitude—a higher amplitude will make the waves unstable and deposit their energy at a lower altitude. Breaking waves will deposit both momentum and energy. The momentum will contribute to changing the wind and driving the circulation while the energy will heat the atmosphere. In GW parameterizations the relation between the momentum deposition and the heat transport is determined by the Prandtl number. The convergence of heat transport is represented by a diffusion coefficient, which is inversely proportional to the Prandtl number (Garcia et al., 2014).

For a model to correctly simulate mesospheric NO abundance, it needs to accurately include all these processes at once: the thermospheric EEP production of NO, the mesospheric production, the transport from the thermosphere across the mesopause (by molecular and eddy diffusion), and the transport mechanisms within the mesosphere. Some of these processes have already been investigated in WACCM.

In a statistical study, Hendrickx et al. (2018) found mesospheric NO to be underestimated in WACCM 4 when compared to observations from SOFIE. They suggested two potential reasons for this: The thermospheric NO density maximum was consistently located 5 km higher in WACCM compared to SOFIE. The descent rate (at 80–100 km altitude) was however found to be the same in model and observations, just that the source of descent is at 110 km in WACCM and 105 in SOFIE. They used a model version without any mesospheric direct production and attributed some of the underestimates to this.

Smith-Johnsen et al. (2018) investigated these two sources of uncertainty further. Including mesospheric NO production in WACCM improved the mesospheric direct production and brought it close to the observations by SOFIE, but a mesospheric underestimate was still found and attributed to the indirect effect. In the same paper, they also investigated the effect of shifting the thermospheric NO production in WACCM down by 5 km. This improved the thermospheric NO in the model during quiet geomagnetic conditions, but a thermospheric underestimation was still present in the model during geomagnetically active times. More importantly, the mesospheric indirect NO effect was not improved by this vertical shift of the thermospheric production altitude.

In the latest model version, WACCM 6, the mesospheric NO underestimate seen in the earlier model version is smaller but still remains. Direct mesospheric production is now accounted for with the inclusion of medium

energy electrons (van de Kamp et al., 2016) and D-region chemistry (Verronen et al., 2016). If the rate of the descent is accurate (Hendrickx et al., 2018), shifting the thermospheric production region down does not improve the mesospheric NO abundance (Smith-Johnsen et al., 2018), does that imply that the mesospheric residual circulation should be shifted higher up? This was also suggested by Smith et al. (2011) who found that WACCM 3.5 underestimated NO descent compared to observations, and attribute it to either (a) the vertical extent of the poleward winter circulation or to (b) the eddy diffusion due to gravity waves is too weak.

To improve the vertical extent of the mesospheric residual circulation, and thereby the NO density profile in WACCM 6, these two sources of uncertainty are investigated in this paper. To vertically shift the mesospheric circulation, the GWs breaking altitude must be adjusted. The initial amplitude of the GW, combined with the background wind and the wavelength, determines where it breaks. As the uncertainties in the sources of non-orographic GWs are larger than those of orographic GWs (Richter et al., 2010), this study will focus on the initial amplitude of the non-orographic GWs (the parameter τ_B in WACCM 6).

To change how the force from breaking GWs is distributed between driving the circulation and eddy diffusion, the ratio between these two, the Prandtl number (Pr) is adjusted. The aim of this paper is to see how these two parameters (τ_B and Pr) are impacting the mesospheric NO and temperature in WACCM 6.

The paper starts with a comparison of WACCM simulations of mesospheric NO and temperature to observations by SOFIE in the southern hemisphere, to highlight where the model is doing well and where improvement is needed (Section 3.1). Section 3.2 investigates model sensitivity to changes in the non-orographic gravity wave amplitude (τ_B) and Section 3.3 to changes in the Prandtl number (Pr), to understand how these parameters impact the NO and temperature vertical profiles. Section 3.4 investigates the position and temperature of the mesopause in the different sensitivity runs compared to SOFIE observations, and Section 3.5 gives a brief view of the same in the northern hemisphere. Section 3.6 gives a more global view by comparing the model results to temperatures from SABER, which measures at all latitudes, not just the polar regions. The discussion (Section 4) interprets and compares these results to recent research before the Conclusion (Section 5) summarizes the findings.

2. Methods

2.1. The Solar Occultation for Ice Experiment (SOFIE)

The Solar Occultation For Ice Experiment (SOFIE) instrument on board NASA's Aeronomy of Ice in the Mesosphere (AIM) satellite was launched in April 2007 and is measuring properties of the mesosphere and lower thermosphere (J. Russell et al., 2009). SOFIE performs solar occultation measurements to retrieve temperature and vertical profiles of NO, among other chemical species (Gordley et al., 2009). The satellite orbit is Sun-synchronous with a period of 96 min, and SOFIE makes measurements twice per orbit, during sunset and sunrise. The 15 measurements in the southern hemisphere are performed during local sunrise (66° S–88° S), and the northern hemispheric measurements are from sunset (65° N–85° N). After 2017 the hemisphere of sunrise and sunset were reversed. The NO measurements are retrieved up to 150 km, with sampling every 0.2 km and a vertical resolution of 1 km. SOFIE has a large vertical range that covers observations from both the mesosphere and lower thermosphere and is ideal for this study. During northern hemispheric summer, SOFIE's measurements are impacted strongly by polar mesospheric clouds. This limitation is not as serious in the southern hemisphere, so the focus of this study will be on the southern hemisphere and the summer NO observations below 80 km have been given less attention. The data is used in this study is version 1.3.

2.2. The Sounding of the Atmosphere Using Broadband Emission Radiometry (SABER)

The Sounding of the Atmosphere using Broadband Emission Radiometry (SABER) instrument is one of four instruments on NASA's (Thermosphere Ionosphere Mesosphere Energetics Dynamics (TIMED) satellite. The satellite was launched in 2001, in a Sun synchronous orbit with a mean orbit period of 97 min. The SABER instrument measures the temperature with an effective vertical resolution of 2 km in the altitude range from 20 to 110 km, and at latitudes 50° S–80°N or 80° S–50°N alternating every 60 days (J. M. I. Russell et al., 1999). The error in the measurements is no more than 2 K below 70 km, while in the upper mesosphere to lower thermosphere region it increases to 6.7 K at 100 km and 25 K at 110 km (Remsberg et al., 2008). The temperature observations used in this study are from the 2.0 version of the SABER data.

2.3. The Whole Atmosphere Community Climate Model (WACCM)

The Whole Atmosphere Community Climate Model (WACCM) is the National Center for Atmospheric Research's global chemistry-climate model and is part of the Community Earth System Model (Hurrell et al., 2013). The model version used in this study is WACCM-D 6 (Gettelman et al., 2019), which extends vertically from the ground to about 140 km geometric height, with 88 pressure levels and horizontal resolution of 1° latitude by 1° longitude. The Specified Dynamics version of WACCM is nudged with reanalysis data from NASA Global Modeling and Assimilation Office's Modern-Era Retrospective Analysis for Research and Applications (Rienecker et al., 2011) by the method described in Kunz et al. (2011), from the surface up to 50 km, with a transition region from 50 to 60 km, and is free running above 60 km.

In WACCM the ionization from auroral electrons (<30 keV) is parameterized by the Kp index. The auroral energy spectrum has a Maxwellian energy distribution with a fixed characteristic energy of 2 keV, which implies that the ionization rate profile will always peak at the same altitude (around 110 km; Roble & Ridley, 1987). There is additionally a NO upper boundary model (NOEM) parameterized by Kp and F10.7 based on NO observations by the Student NO Experiment satellite (SNOE; Marsh et al. [2004]). WACCM 6 differs from older model versions as it also includes ionization from radiation belt electrons (referred to as Medium Energy Electrons [MEE] in the atmospheric community). MEE ionization is parameterized by the Ap index and is based on observations from the MEPED instrument (van de Kamp et al., 2016).

Extra chemistry has been implemented in the updated model (D-region chemistry) which leads to the production of NO also in the mesosphere. The new chemical scheme is based on a simplification of the Sodankylä Ion Chemistry one-dimensional model (Verronen et al., 2016), with only the most important chemical reactions included based on their effects on the mesosphere (Verronen & Lehmann, 2013)). Where WACCM 4 included the five major ions in the thermosphere, WACCM 6 includes these five and has in addition 20 positive ions and 21 negative which enables 307 new ion reactions in the mesosphere. This allows for NO production by EEP the same way as in the thermosphere and also through multiple cluster ion-ion re-combinations or by positive ion reactions in the mesosphere. The ion chemistry is included in WACCM over the whole altitude range, but the positive ion clusters and negative ions are less abundant above 90 km, and their effect becomes less important in the thermosphere where the standard WACCM chemistry is still dominating (Verronen et al., 2016).

The mesospheric circulation is driven by gravity waves propagating up from the troposphere. What separates WACCM 6 from many other models, is that it includes both an orographic GW parameterization (McFarlane, 1987) and a non-orographic GWs (Richter et al., 2010). A spectrum of non-orographic GWs is launched from 600 hPa (~4 km) when the frontogenesis exceeds a certain threshold value (Richter et al., 2010). The amplitudes of the waves in the spectrum vary with a fixed Gaussian shape that has a peak amplitude of τ_B. The frontogenesis threshold has been updated in WACCM 6 due to the change in resolution to $0.108\ K^2(100\ km)^{-2}h^{-1}$, and the amplitude of the non-orographic gravity waves at the source level is set to $2.5 \cdot 10^{-3}\ Pa$ (Gettelman et al., 2019). The Prandtl number, which determines the relation of eddy diffusion and momentum forcing from the GW breaking, is Pr = 2 in WACCM 6. This is an update from WACCM 4 where it was Pr = 4, meaning the eddy diffusion has been increased in the current model version compared to previous versions (as the turbulent Prandtl number is inversely proportional to the eddy diffusion).

2.4. WACCM Model Runs

To investigate the effect of GWs on the temperature and NO distribution in the MLT region, five WACCM runs have been performed with different specifications of the non-orographic gravity wave amplitude (τ_B) and Prandtl number (Pr). All model runs are performed with WACCM 6, with D-region chemistry, low and medium energy electron precipitation according to the CMIP6 recommendation, and using the specified dynamics mode (FWmadSD). The model data is output at the SOFIE measurement locations, 15 times each day, and has then been converted into daily averages. The same has been done for the SABER comparison. All data shown, from both WACCM, SOFIE, and SABER, are from the year 2010. An overview of the difference in the five model runs are shown in Table 1.

Table 1
Overview of Setting for the Five Model Runs, the Only Differences Between Them Are the Value of the Non-Orographic Gravity Wave Starting Amplitude, and the Prandtl Number

Model run	Amplitude (τ_B)	Prandtl number (Pr)	Color in figures
Standard WACCM	$2.5 \cdot 10^{-3}$	2	Purple
Lower amplitude $\left(\cdot\frac{1}{5}\right)$	$5.0 \cdot 10^{-4}$	2	Red
Higher amplitude ($\cdot 5$)	$1.25 \cdot 10^{-2}$	2	Orange
Less eddy diffusion $\left(\cdot\frac{1}{2}\right)$	$2.5 \cdot 10^{-3}$	4	Green
More eddy diffusion ($\cdot 2$)	$2.5 \cdot 10^{-3}$	1	Blue

3. Results

3.1. Mesospheric NO and Temperature in WACCM and SOFIE

NO simulated by WACCM and observed by SOFIE show many similarities and some differences (upper panels of Figure 1). The general features are the same in the model run and the observations: NO vmr is increasing exponentially with altitude throughout the mesosphere and lower thermosphere, from about 1 ppmv at the stratopause to 10^3 ppmv at mesopause. The highest values are found in the thermosphere during geomagnetic activity. During winter, more thermospheric NO is transported down to the lower mesosphere leading to 10 times higher values than during summer. Some differences are also found (upper right panel of Figure 1). WACCM thermospheric NO during summer is higher than in the SOFIE observations (+50% during January-March and October-December in the altitude region 90–115 km). During winter more variation is seen in the thermospheric NO difference, but on average WACCM shows less than SOFIE (−35% in April-September in the altitude region 90–115 km). As summer observations of mesospheric NO can be contaminated by the presence of polar mesospheric clouds, they will not be used directly for model validation. During mesospheric winter WACCM shows significantly lower values of NO than what is observed by SOFIE (−75% at 55–90 km). In summary, the modeled lower thermospheric summer NO is overestimated, while in winter the modeled NO is underestimated throughout the MLT.

The temperature simulated with WACCM shows similar features to what SOFIE observes, but when directly compared also differ from the observations (lower panels of Figure 1). The modeled thermospheric summer temperatures are warmer than observations (+30 K at 90–105 km). During winter the difference in temperature is more varying but shows more or less the same in model and observation (±10 K at 90–105 km). Summer mesospheric temperatures are colder in WACCM than in observations (−20 K at 55–90 km). During mesospheric

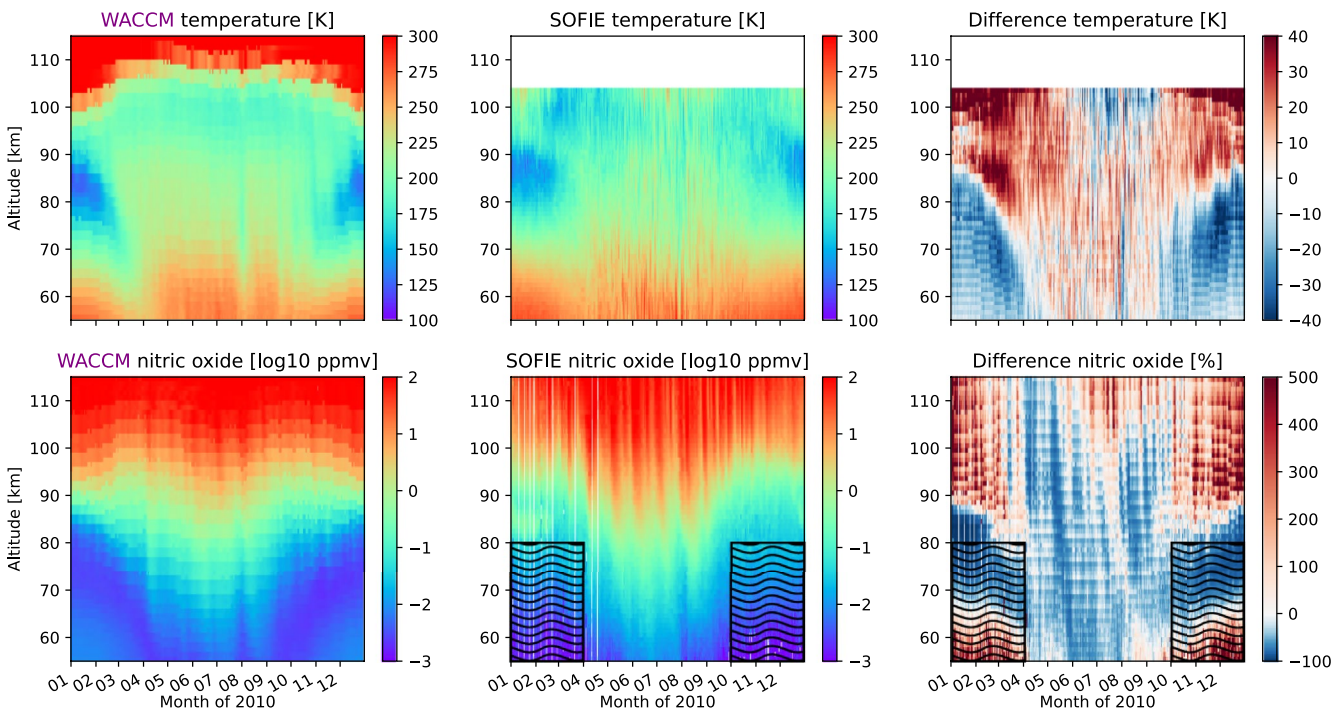

Figure 1. Upper panels: Temperature [K] from Whole Atmosphere Community Climate Model (WACCM), and Solar Occultation For Ice Experiment (SOFIE), and the difference between them (WACCM-SOFIE [K]). Lower panels: Nitric oxide volume mixing ratio [log10 ppmv] from WACCM, and SOFIE, and the relative difference between them (WACCM-SOFIE/WACCM [%]). All figures are daily averages, from the southern hemisphere, the year 2010, and the WACCM data is co-located with the observations from SOFIE. Mesospheric summer observations of NO by SOFIE can be contaminated by polar mesospheric clouds, so this region is shaded and given less attention.

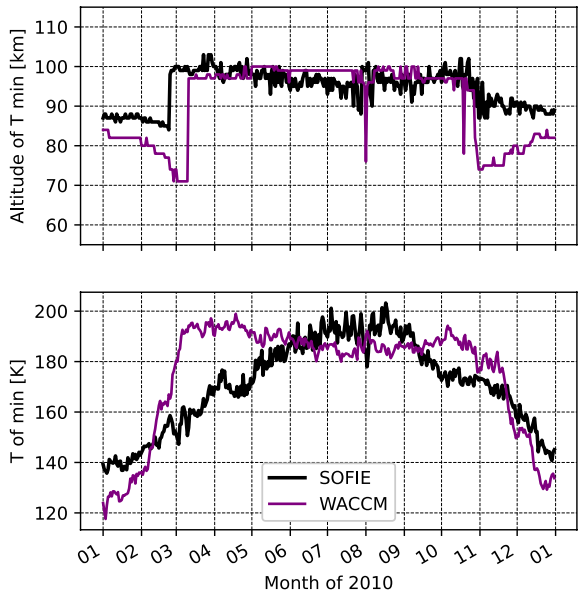

Figure 2. Upper panel: The temporal evolution of mesosopause altitude [km]. Lower panel: The mesopause temperature [K]. Both in the southern hemisphere in 2010. Whole Atmosphere Community Climate Model (purple) compared to SOFIE (black) shows that some of the temperature discrepancies are due to a vertically displaced summer mesopause and a temporal offset in the summer to winter reversal.

winter, WACCM is closer to SOFIE (±10 K at 55–90 km). Summarized, the modeled summer temperatures shows the largest discrepancies, while during winter where the NO is underestimated, only small differences are seen in temperature.

Comparing the mesopause altitude in WACCM to SOFIE highlights part of the reason for the temperature discrepancies seen (upper panel of Figure 2). The altitude of the mesopause in WACCM is lower in SH summer (−5 to 15 km), and the transition from summer to winter occurs later than in SOFIE (mid February in SOFIE, mid March in WACCM). The largest temperature difference is found in early March when the mesopause in SOFIE has shifted to winter position while WACCM is still in summer. The time of the summer to winter circulation is also when the temperature difference at the mesopause (lower panel of Figure 2) between WACCM and SOFIE is the largest (+20–30 K). In the summer WACCM has a colder mesopause than SOFIE (−10–15 K). The winter mesopause temperature is similar in WACCM and SOFIE (±10K). The observed temperature at the mesopause changes more gradually, while the modeled mesopause temperature displays a more sudden jump from summer to winter temperature. The largest differences found in temperature are thus due to a displaced summer mesopause.

3.2. NO and Temperature Sensitivity to Non-Orographic Gravity Wave Amplitude

Changing the amplitude of the non-orographic gravity waves will change their breaking altitude which impacts both temperature and transport of nitric oxide. WACCM 6 has the amplitude set as $\tau_B = 2.5 \cdot 10^{-3}$. In two sensitivity runs where all else is the same, this value is reduced to a fifth of the original ($\tau_B = 5 \cdot 10^{-4}$, red), and increased to five times the original value ($\tau_B = 1.25 \cdot 10^{-2}$, orange) as listed in Table 1.

Compared to the standard WACCM run, both temperature and NO change due to the reduced amplitude (left panels of Figure 3). The summer thermosphere is cooler (−30 K at 90–100 km), and so is the winter lower mesosphere (−15 K at 55–65 km). The other regions are warmer (+10 K at 55–85 km in summer, +5 K in 65–105 km in winter, and +15 K at 105–115 km in winter). Less NO is found in the summer mesosphere (−30% at 55–90 km) due to the reduced amplitude. The biggest increase is seen during winter at the mesopause and below (+30% 55–100 km), strongest during late winter in the lower mesosphere (+200% at 55–75).

Increasing the amplitude leads to the opposite response in both temperature and NO (right panels of Figure 3). The mesospheric NO response is increased during summer and decreases during winter. Compared to SOFIE more NO was needed during winter, especially in the mesosphere. Increasing the amplitude does the opposite and brings the model even further away from observations.

An altitude by altitude comparison of nitric oxide from these model runs to SOFIE observations is shown in Figure 4. Reducing the non-orographic gravity wave amplitude (τ_B) brings more NO down to the mesosphere during winter (red line in Figure 4) and 4 the model run that improves the wintertime mesospheric NO the most.

3.3. NO and Temperature Sensitivity to the Prandtl Number

The Prandtl number is set to Pr = 2 in WACCM 6. The effect of a doubling (Pr = 4, green, less eddy diffusion) and halving (Pr = 1, blue, more eddy diffusion) of this number is compared to standard WACCM. Decreasing eddy diffusion (left panels of Figure 5) warms the thermosphere, where WACCM already was too warm compared to SOFIE. Less NO is found in the mesosphere where WACCM already had a deficit.

Increasing eddy diffusion (right panels) cools the thermosphere significantly (−20 K from the mesopause and above). Below the mesopause, in SH summer there is slight warming and a wintertime cooling, though more fluctuating and with lower values (±10 K). More eddy diffusion leads to more NO at all altitudes. In the thermosphere, the enhancement is smallest, and seems seasonally independent (+20% at 90–115 km annual

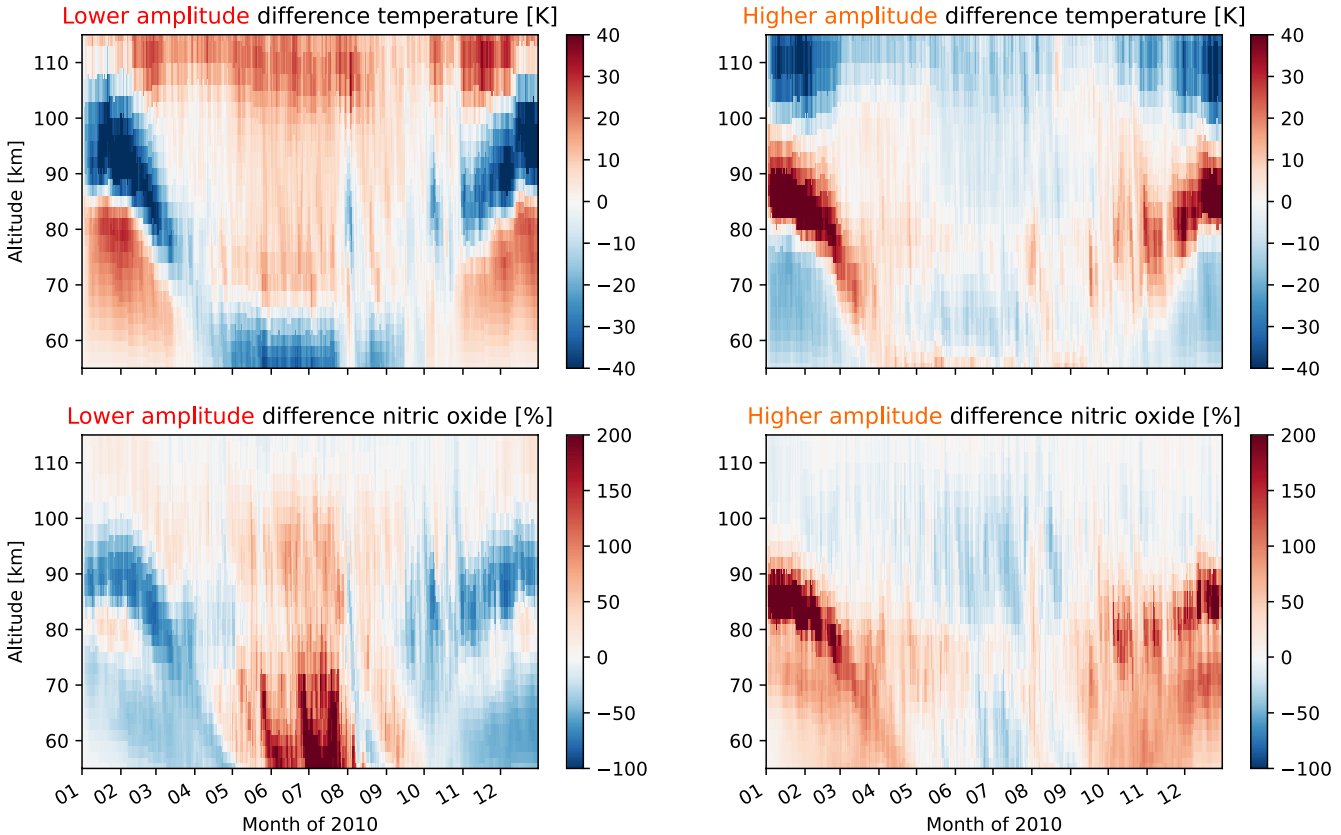

Figure 3. Upper panels: Change in temperature [K] by changing the gravity wave amplitudes (τ_B). Lower panels: Change in NO [%]. Both are relative to the standard Whole Atmosphere Community Climate Model run. Difference when decreasing the τ_B to $\frac{1}{5}$ (left), and by increasing it by a factor of 5 (right). The amplitude change shifts the vertical temperature distribution and impacts how much NO is transported up during summer and down during winter.

average). Short periods of NO decrease are seen in the thermosphere during high geomagnetic activity (−10% at 90–115 km). In the upper mesosphere, there is a strong NO increase, and during winter this enhancement also reaches the lower mesosphere (+135% at 55–90 km).

A direct comparison of the NO from the eddy diffusion sensitivity runs to SOFIE is shown in Figure 6). The increased diffusion run (blue line) improves the modeled NO from the standard run (purple line) when compared to SOFIE (black line). Additional tuning is needed, as the modeled NO now overshoots a bit compared to observations.

3.4. The Impact on the Mesopause Altitude and Temperature

The altitude and temperature of the mesopause changes in the sensitivity runs (Figure 7). The amplitude of the non-orographic gravity waves in WACCM determines at what altitude these waves will deposit their energy. Reducing the amplitude allows the waves to propagate to higher altitudes before they break, and this shifts the altitude of the mesopause higher up. By reducing the amplitude to a fifth of the original (from the purple line in Figure 7 to the red line), the mesopause is lifted about 10 km during summer, closer to the SOFIE observed mesopause altitude (black line). The transition from summer to winter is postponed by 14 days compared to the original model run, which was already late compared to the observations. The winter mesopause altitude does not change considerably. Increasing the amplitude by five times (to the orange line), lowers the summer mesopause altitude further away from the observed altitude. The higher amplitude run does however start the transition to summer 14 days earlier, which is closer to observations. The winter mesopause altitude is not changed in the amplitude runs but was already similar to observations. The temperature of the mesopause changes when the gravity wave amplitude is changed (lower left in 7). A lower amplitude reduces the summer mesopause temperature and increases the winter temperature.

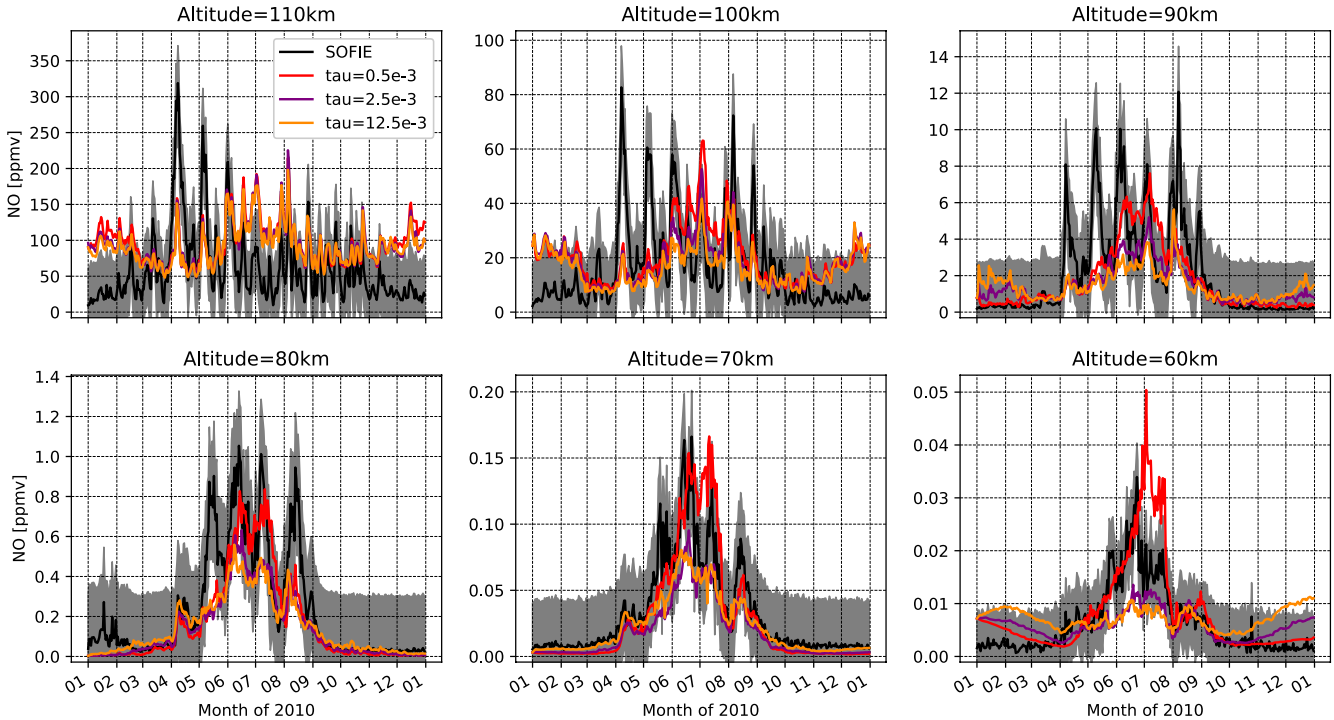

Figure 4. The effect of changing the non-orographic gravity wave amplitude (τ_B) on the temporal evolution of mesospheric and lower thermospheric nitric oxide [ppb], altitude by altitude, in the southern hemisphere in 2010. Whole Atmosphere Community Climate Model (WACCM) with reduced gravity wave amplitude (red) and WACCM with increased amplitude (orange), contrasted by WACCM standard (purple) and observations from Solar Occultation For Ice Experiment (black).

Changing the Prandtl number in WACCM does not change the altitude of the mesopause (upper right panel in 7), but a significant change is seen in the temperature of the mesopause (lower right panel in 7). Reducing the eddy diffusion to half of the original (from the purple line to the green) does not impact the summer mesopause altitude or temperature, but during winter this significantly increases the temperature at the mesopause. Doubling the eddy diffusion (blue line) decreases the winter mesopause temperature, which is further away from the observed temperatures by SOFIE.

3.5. Northern Hemispheric Mesopause Altitude and Temperature

The differences in NO between SOFIE and WACCM identified for the SH are also seen in the not shown (NH), though the satellite altitude range is more limited due to the presence of polar mesospheric clouds during northern summer. SOFIE temperature observations of the mesopause altitude and temperature are however trustworthy also in the north and can be used to validate the model runs. Figure 8 shows similar results to what was found in the SH in Figure 7: The summer mesopause is located at a lower altitude in WACCM (purple line) than in SOFIE (black line). This is improved by reducing the amplitude of the gravity waves (red line). The winter mesopause temperature (lower panels) is warmer in WACCM (purple line) than in SOFIE (black line), but improved by increasing the eddy diffusion (blue). The shape of the modeled mesopause temperature evolution fits better to observations in the north than what was found for the south.

3.6. Global View of Temperature Effects

The results found in the previous sections do not only apply in the small latitudinal region where SOFIE is measured. SABER observes temperatures at all latitudes and gives a similar picture to SOFIE. Looking at averages of the NH summer months (June 21st to September 23rd) in Figure 9 similar features are seen in WACCM (upper left panel) as in SABER (upper right panel).

The lower panels show the temperature difference between SABER and WACCM (WACCM - SABER) for the standard run (left panel in the second row). The largest differences are found toward the summer pole, where the

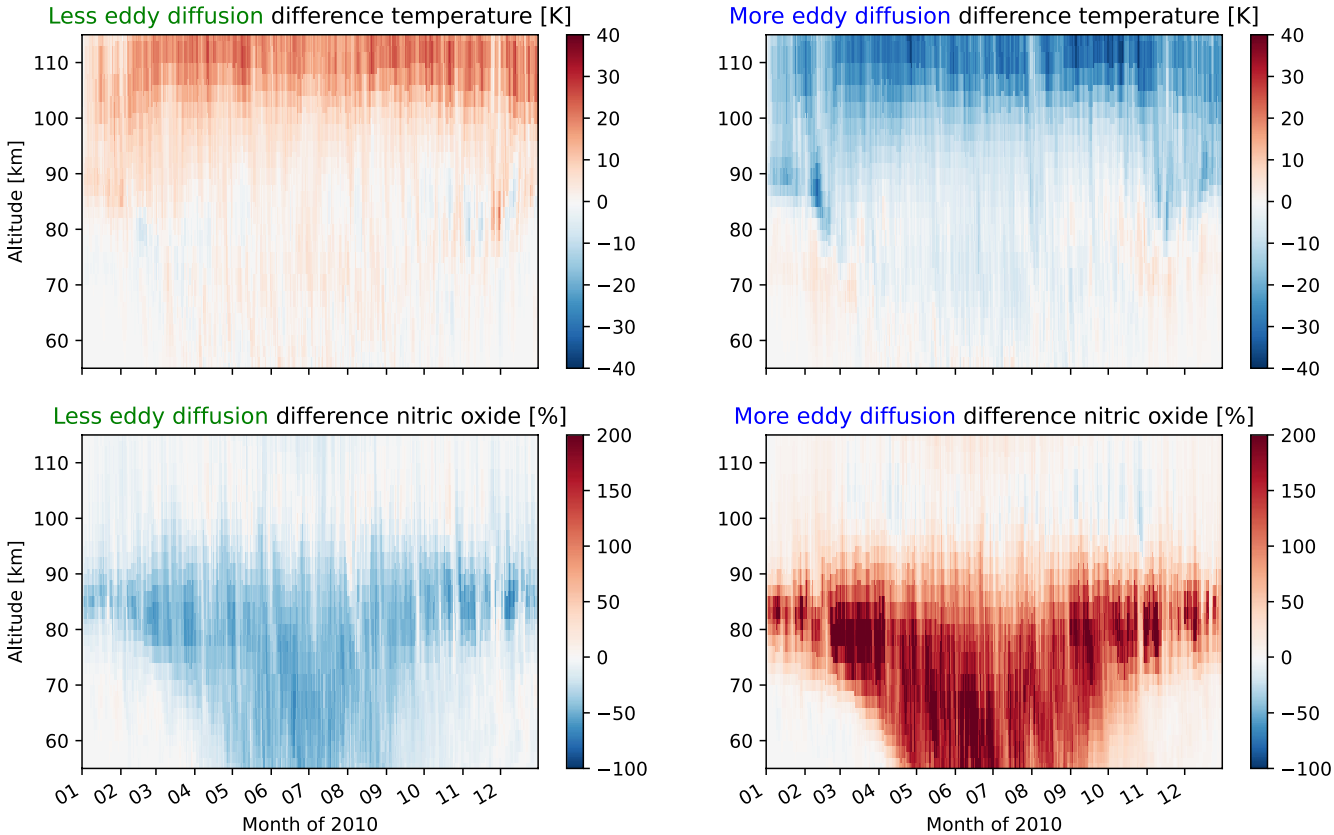

Figure 5. Upper panels: Change in temperature [K] by changing the Prandtl number (Pr). Lower panels: Change in nitric oxide (NO) [%]. Both are relative to the standard Whole Atmosphere Community Climate Model run. The difference when decreasing the eddy diffusion by increasing the Prandtl number to Pr = 4 (left), and increasing eddy diffusion by setting Pr = 1 (right). The Prandtl number changes the thermospheric temperature and the amount of mesospheric NO.

modeled temperature is too cold in WACCM in the mesosphere, and around the mesopause where it is too warm. At all latitudes, the modeled lower thermosphere is too warm.

The difference is reduced when SABER is compared to the two best sensitivity runs; the lower amplitude run (middle lower panel) and the increased diffusion run (right lower panel). Lowering the amplitude reduces the cold mesosphere and the warm mesopause. The warm bias in the lower thermosphere remains. The increased diffusion run, on the other hand, improves the lower thermosphere bias but does not improve the mesopause and mesosphere as much.

Looking at the NH winter months (December 21st to March 20th) in Figure 10, these same results hold for when the summer pole is in the south. The temperature biases are however stronger here than in the north, while the thermospheric warm bias is about the same.

The vertical shift of the summer mesopause in WACCM that was identified compared to SOFIE is also seen by SABER. Figure 11 upper panels show the mesopause altitude in SABER (black) compared to standard WACCM (purple), the decreased amplitude run (red), and the increased diffusion run (blue). While SOFIE showed this feature for only a limited latitude range, SABER shows that this shift occurs at both poles, starting at mid latitudes (5–10 km at 30–75°). The reduced amplitude run improves the location of the mesopause for both summer hemispheres, while the increased diffusion does not change the altitude, as was also found using SOFIE observations.

The lower panels of Figure 11 show the temperature at the mesopause. Here the increased eddy diffusion run lowers the mesopause temperature at low latitudes and brings it closer to SABER observations. The modeled winter pole temperature bias is significantly stronger in the SH than in the NH.

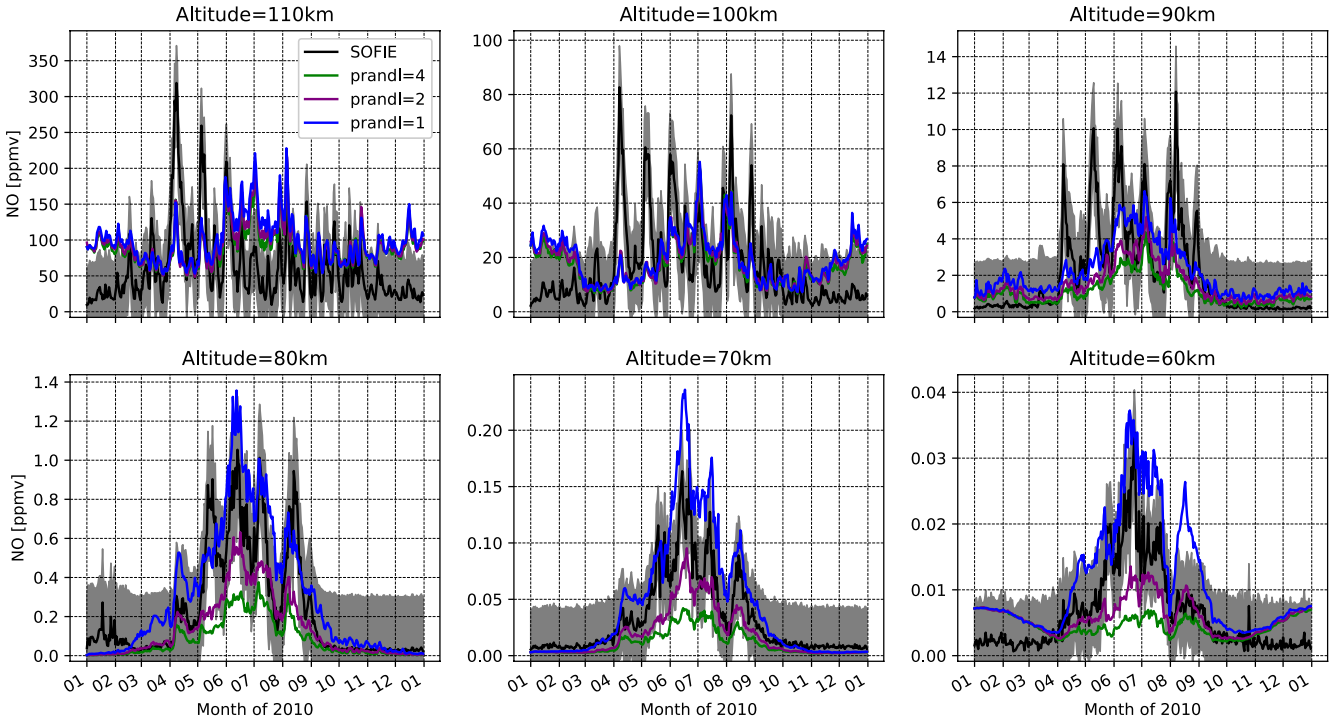

Figure 6. The effect of changing the Prandtl number (Pr) on the temporal evolution of mesospheric and lower thermospheric NO [ppb], altitude by altitude, in the southern hemisphere in 2010. Whole Atmosphere Community Climate Model (WACCM) with reduced eddy diffusion (green) and WACCM with increased eddy diffusion (blue), contrasted by WACCM standard (purple) and observations from Solar Occultation For Ice Experiment (black).

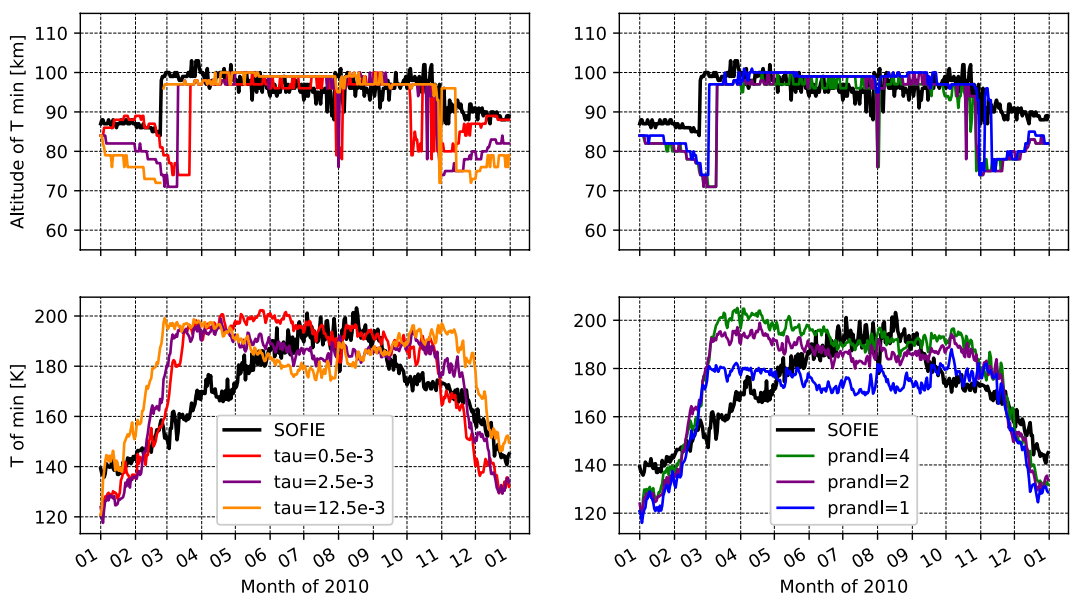

Figure 7. The temporal evolution of mesosopause altitude [km] and mesopause temperature [K], in the southern hemisphere in 2010. Solar Occultation For Ice Experiment (black), compared to Whole Atmosphere Community Climate Model (WACCM) with different gravity wave drag settings: standard WACCM (purple, $\tau_B = 2.5 \cdot 10^{-3}$, Pr = 2), WACCM with reduced gravity wave amplitude (red, $\tau_B = 5.0 \cdot 10^{-4}$), WACCM with increased gravity wave amplitude (yellow, $\tau_B = 1.25 \cdot 10^{-2}$), WACCM with reduced eddy diffusion (green, Pr = 4), and WACCM with increased eddy diffusion (blue, Pr = 1). Amplitude affects mesopause summer altitude and eddy diffusion changes mesopause winter temperature.

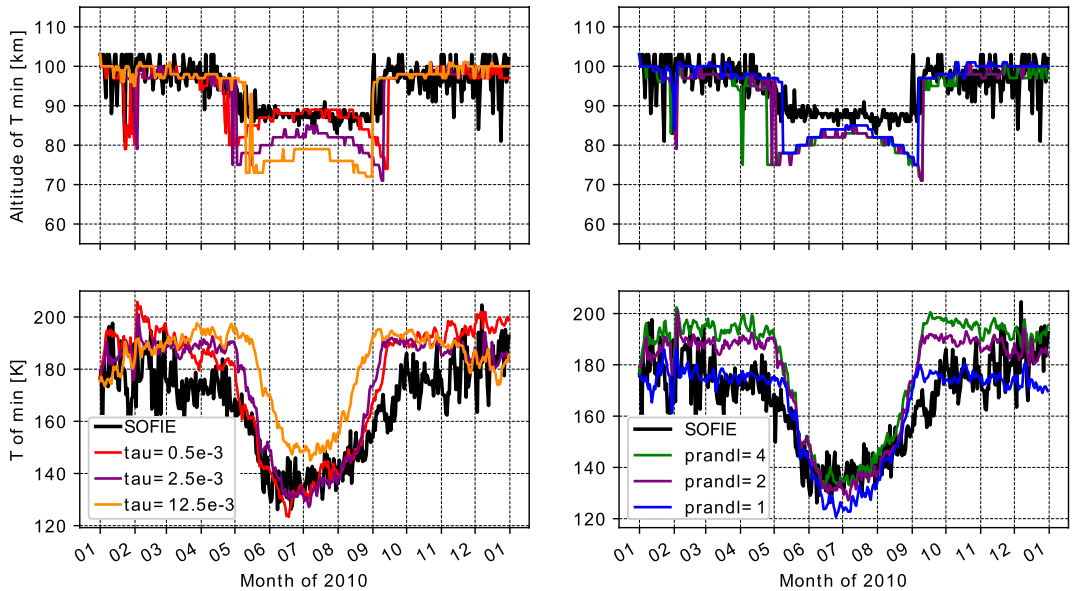

Figure 8. Northern hemispheric mesopause altitude and temperature, complementing the Southern hemispheric results from Figure 7. The temporal evolution of mesopause altitude [km] and mesopause temperature [K], in the northern hemisphere in 2010. Solar Occultation For Ice Experiment (black), compared to Whole Atmosphere Community Climate Model (WACCM) with different gravity wave drag settings: standard WACCM (purple, $\tau_B = 2.5 \cdot 10^{-3}$, Pr = 2), WACCM with reduced gravity wave amplitude (red, $\tau_B = 5.0 \cdot 10^{-4}$), WACCM with increased gravity wave amplitude (yellow, $\tau_B = 1.25 \cdot 10^{-2}$), WACCM with reduced eddy diffusion (green, Pr = 4), and WACCM with increased eddy diffusion (blue, Pr = 1). Amplitude affects mesopause summer altitude and eddy diffusion changes mesopause winter temperature.

4. Discussion

When the distribution of NO simulated by WACCM 6 is compared to observations from SOFIE, the modeled wintertime NO is found to be underestimated in the mesosphere. The same result was found by Hendrickx et al. (2018) looking at 10 years of SOFIE measurements compared to WACCM 4, and by Smith-Johnsen et al. (2018) which investigated one particularly strong geomagnetic storm in 2010. The summertime temperature in the model is too high in the thermosphere and too low in the mesosphere. This difference is partly attributed to vertically displaced summer mesopause in the model. Smith (2012) found a similar altitude shift in mesopause from WACCM 3.5 compared to SABER temperature climatologies. The discrepancy in temperature between model and observations indicates deficiencies in the model dynamics, and the NO underestimate in the winter mesosphere is hence more likely due to insufficient transport than insufficient production of NO.

A potentially improved representation of the indirect effect needs to be validated by a better modeled temperature, position of the mesopause, and the timing of the seasonal transition. The sensitivity model runs show that both a lower GW amplitude or increased eddy diffusion will increase the amount of NO reaching the winter mesosphere. Decreasing the amplitude lifts the summer mesopause up to the altitude where the observed mesopause is. The smaller amplitude GWs are able to propagate higher up before they break. Their energy and momentum will be deposited at a higher altitude, which will shift the vertical extent of the advection higher up. Smith et al. (2011) suggested that the GW breaking altitude was too low in WACCM3.5, and our finding supports their conclusion.

Although a reduction in the GW amplitude strengthens the indirect effect on NO and altitude of the summer mesopause, the delayed seasonal transition raises doubt if a lower amplitude alone gives a more realistic representation of the true dynamics of the MLT. The seasonal transition is forced from below and all the sensitivity runs are constrained by the same re-analysis data. A shift in the seasonal transition reflects the GWs ability to transfer the signal into the MLT region, a longer delay suggests that the wave forcing is too weak in the lower mesosphere when reducing the GW amplitude. Therefore, it is not possible to exclude that the vertical shift imposed by changing the GW amplitude ought to be reached by alternative ways of tuning the parameterization such as for example, modifying the gravity wave spectrum itself. This is also confirmed by the increased amplitude run,

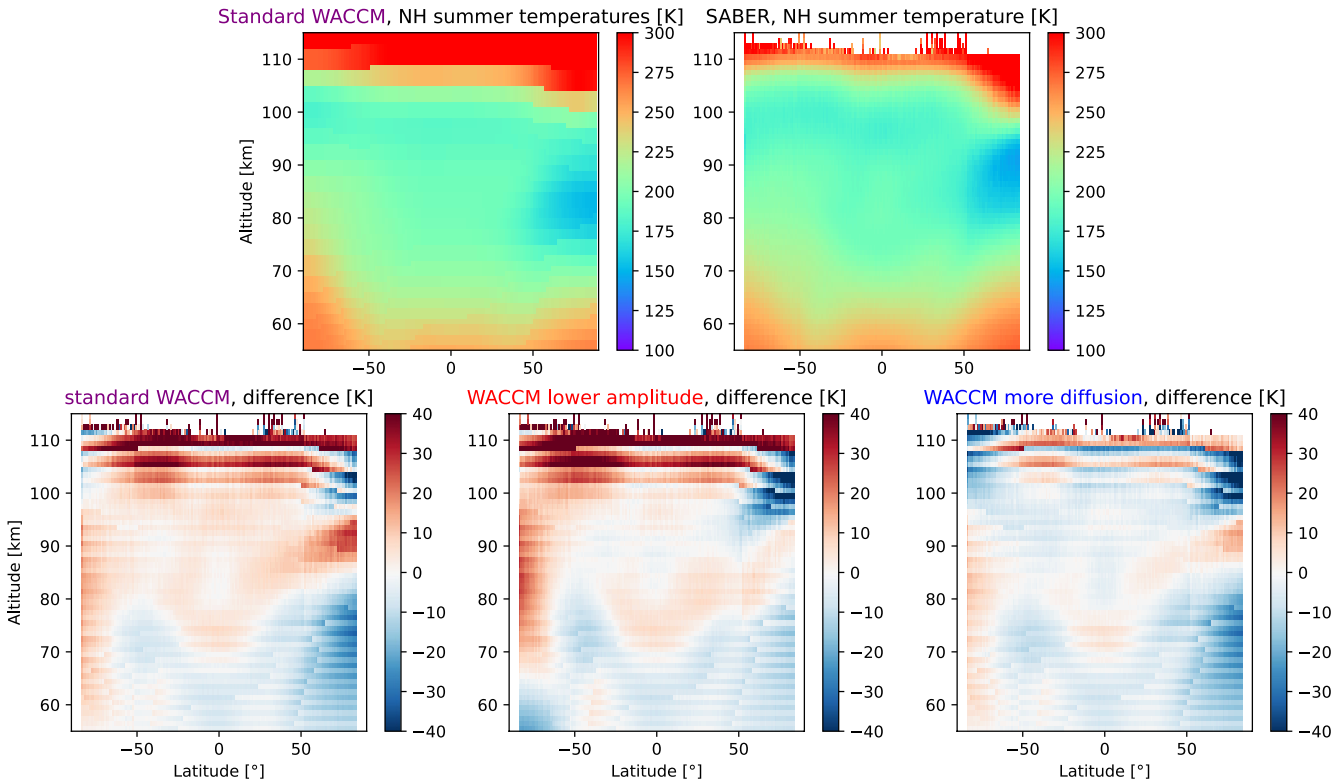

Figure 9. Upper panels: Temperature [K] from Whole Atmosphere Community Climate Model (WACCM), and The Sounding of the Atmosphere using Broadband Emission Radiometry (SABER), distributed over latitudes (rather than time as it was for Solar Occultation For Ice Experiment). Average over the NH summer months (June 21st to September 23rd). Lower panels: The difference between WACCM and SABER (WACCM-SABER) [K]. In the left panel SABER is compared to the standard WACCM run ($\tau_B = 2.5 \cdot 10^{-3}$, Pr = 2), the middle panel shows the comparison to the reduced amplitude run ($\tau_B = 5.0 \cdot 10^{-4}$), and the right panel shows SABER compared to the increased eddy diffusion run (Pr = 1).

which reduced the amount of NO reaching the mesosphere and shifts the mesopause altitude deeper down, but still, get the seasonal transition at the same time as SOFIE observations.

The increased eddy diffusion run increases the amount of NO reaching the mesosphere, by mixing in more of the NO-rich thermospheric air with the mesospheric air where it is captured by the residual circulation. Reduced eddy diffusion will distribute more of the GW breaking energy to drive the circulation and less to turbulence. The increased downwelling associated with the reduced eddy diffusion has however a smaller impact on the NO transport than the the increased mixing from the increased eddy diffusion run. Using the HAMMONIA model Meraner and Schmidt (2016) found little effect of eddy diffusion compared to molecular diffusion and advection. Their conclusion was based on a Prandtl number Pr = 3, and when reducing it to Pr = 1.5 they found an increased NO transport similar to what is found in this study.

The processes discussed in our study are not the only possible causes of the discrepancies seen. Validating the model results by only the observable effect on NO and temperature rather than by observations of the GW themselves is a limitation. Due to the small spatial scale of large parts of the gravity wave spectrum, constraining gravity wave drag from global satellite observations unfortunately still remain a challenge (Geller et al., 2013). Also, the satellite coverage will limit the possibility of model validation in time and space. There are other transport processes not investigated here too. The effective transport of NO by molecular diffusion is important above the mesopause (Meraner et al., 2016; Smith et al., 2011), the effect from tides have not been looked into, and the effects from the orographic gravity waves have not been investigated.

The amount of NO in the mesosphere is a combination of local production and transport from other source regions. In this study, only transport has been considered. There are however uncertainties in production too. Thermospheric production in WACCM is found to be too high during quiet geomagnetic conditions, too low during storms, and at the wrong altitude compared to satellite observations (Hendrickx et al., 2018; Smith-Johnsen

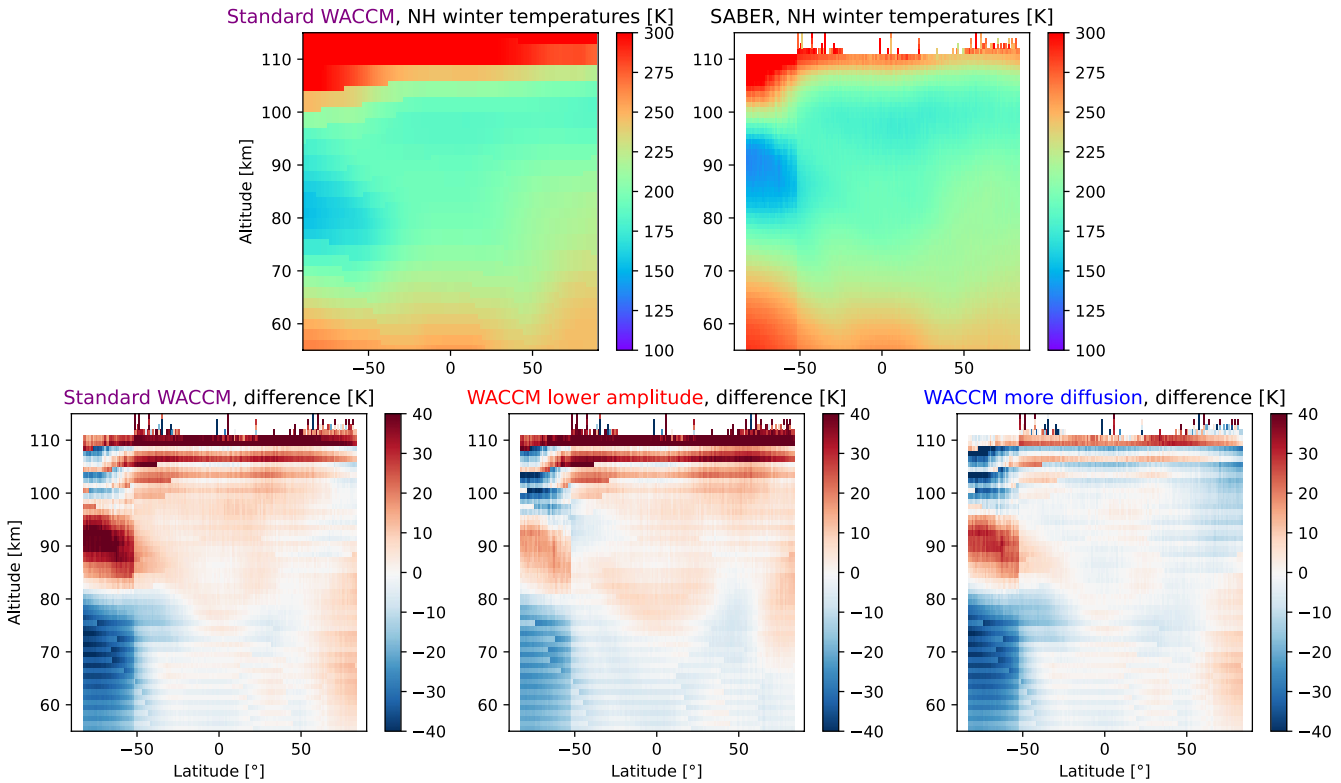

Figure 10. Upper panels: Temperature [K] from Whole Atmosphere Community Climate Model (WACCM), and The Sounding of the Atmosphere using Broadband Emission Radiometry (SABER), distributed over latitudes (rather than time as it was for Solar Occultation For Ice Experiment). Average over the NH winter months (December 21st to March 20th). Lower panels: The difference between WACCM and SABER (WACCM-SABER) [K]. In the left panel SABER is compared to the standard WACCM run ($\tau_B = 2.5 \cdot 10^{-3}$, Pr = 2), the middle panel shows the comparison to the reduced amplitude run ($\tau_B = 5.0 \cdot 10^{-4}$), and the right panel shows SABER compared to the increased eddy diffusion run (Pr = 1).

et al., 2018). These discrepancies will be able to propagate down to the mesosphere during winter and will affect the mesospheric NO level. Local mesospheric production is now included in WACCM 6 (van de Kamp et al., 2016; Verronen et al., 2016), but several studies indicate that the current parameterization is an underestimate compared to other available data sets of mesospheric electron ionization (Nesse Tyssøy et al., 2019; Tyssøy et al., 2021).

5. Conclusion

The vertical distribution of NO in the MLT region is dependent on both production and transport. While production by EEP dominates in the thermosphere, the dynamics are the most important in the mesosphere. Comparing WACCM simulations of NO to SOFIE observations, a modeled wintertime NO underestimate is found in the mesosphere. The direct NO production in the mesosphere is captured by the model, but the transported NO is not. The winter temperatures show reasonable agreement between model and SOFIE observations. In the summer, however, a larger temperature difference is seen, mostly due to a vertical displacement of the mesopause in the model. This is also seen when WACCM is compared to temperature observations by SABER at a larger latitude range. The mesospheric circulation is driven by gravity waves, and by changing where and how the wave energy and momentum are deposited in WACCM, the modeled circulation can be altered to improve both the summer temperature and the winter NO distribution in the MLT region.

When the amplitude of the non-orographic gravity waves in WACCM is reduced, the summer mesopause in WACCM is moved to higher altitudes which fits better with both SOFIE and SABER temperature observations. This brings modeled summer temperatures closer to observations throughout the MLT region. By allowing the waves to break at higher altitudes, more of the high altitude NO rich air is transported down to the

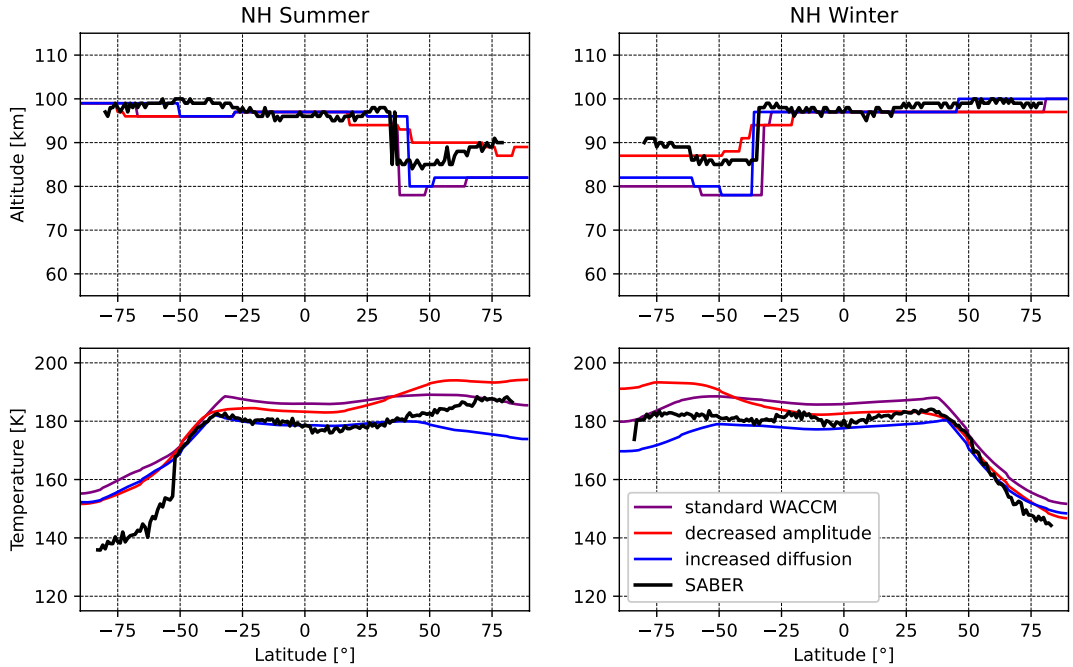

Figure 11. The latitudinal variation of the mesopause altitude [km] and mesopause temperature [K] for NH summer (left) and NH winter (right) in 2010. The Sounding of the Atmosphere using Broadband Emission Radiometry (black), compared to Whole Atmosphere Community Climate Model (WACCM) with different gravity wave drag settings: standard WACCM (purple, $\tau_B = 2.5 \cdot 10^{-3}$, Pr = 2), WACCM with reduced gravity wave amplitude (red, $\tau_B = 5.0 \cdot 10^{-4}$), and WACCM with increased eddy diffusion (blue, Pr = 1). The decreased amplitude improves the summer mesopause altitude and the increased eddy diffusion lowers mesopause temperature.

mesosphere during winter improving the modeled underestimate. Increasing the amplitude does the opposite, but still improves the timing of the summer to winter transition.

The Prandtl number determines how much eddy diffusion is associated with the momentum forcing from the breaking or dissipating gravity wave. By reducing the Prandtl number, the amount of eddy diffusion is increased. The increased eddy diffusion cools the thermosphere and the mesopause, bringing it closer to SOFIE and SABER observations. More turbulence will mix in more NO-rich air from the thermosphere and transport it down to the mesosphere during winter. An increase in diffusion reduces the vertical gradient and therefore reduces the effectiveness of NO transport by the resolved circulation.

This sensitivity study shows that both reducing the amplitude of the non-orographic GWs and increasing the eddy diffusion (by decreasing the Prandtl number) allows for more of the wintertime thermospheric NO to reach the mesosphere where the model was underestimating compared to observations. The improvement in temperature at the same time confirms that these parameters should be updated to improve the modeled dynamics and thus the indirect EEP effect on NO in the MLT region. The reduced amplitude run (red line in figures) shows best agreement with the altitude of the summer mesopause, while the increased diffusion run (blue in figures) gives a more accurate winter mesopause temperature. Both improve the modeled NO transport, though additional tuning is still needed for the transport to be fully captured by the model.

Data Availability Statement

The AIM-SOFIE observations can be downloaded from http://sofie.gats-inc.com/getdata, TIMED-SABER data is accessible from http://saber.gats-inc.com/data.php, and WACCM is freely available from https://escomp.github.io/CESM/versions/cesm2.2/.

Acknowledgments
This study is supported by the Norwegian Research Council under grants 223,252, 302,040, and 300,724. We to thank both reviewers for good suggestions that significantly improved the discussion and content of the paper.

References

Arsenovic, P., Rozanov, E., Stenke, A., Funke, B., Wissing, J. M., Mursula, K., et al.(2016). The influence of middle range energy electrons on atmospheric chemistry and regional climate. *Journal of Atmospheric and Solar-Terrestrial Physics*, *149*, 180–190. https://doi.org/10.1016/j.jastp.2016.04.008

Barth, C. A., Mankoff, K. D., Bailey, S. M., & Solomon, S. C. (2003). Global observations of nitric oxide in the thermosphere. *Journal of Geophysical Research: Space Physics*, *108*(A1), 1027. https://doi.org/10.1029/2002JA009458

Brasseur, G. P., & Solomon, S. (2005). *Aeronomy of the middle atmosphere*. Springer.

Cravens, T. E., Gérard, J.-C., LeCompte, M., Stewart, A. I., & Rusch, D. W. (1985). The global distribution of nitric oxide in the thermosphere as determined by the atmosphere explorer d satellite. *Journal of Geophysical Research: Space Physics*, *90*(A10), 9862–9870. https://doi.org/10.1029/JA090iA10p09862

Crutzen, P. J. (1979). The role of no and no2 in the chemistry of the troposphere and stratosphere. *Annual Review of Earth and Planetary Sciences*, *7*(1), 443–472. https://doi.org/10.1146/annurev.ea.07.050179.002303

Crutzen, P. J., Isaksen, I. S. A., & Reid, G. C. (1975). Solar proton events: Stratospheric sources of nitric oxide. *Science*, *189*(4201), 457–459. https://doi.org/10.1126/science.189.4201.457

Eliassen, N. A., & Palm, E. (1961). On the transfer of energy in stationary mountain waves. *Geofysiske Publikasjoner*, *22*(3).

Eyring, V., Bony, S., Meehl, G. A., Senior, C. A., Stevens, B., Stouffer, R. J., & Taylor, K. E. (2016). Overview of the coupled model intercomparison project phase 6 (cmip6) experimental design and organization. *Geoscientific Model Development*, *9*(5), 1937–1938. https://doi.org/10.5194/gmd-9-1937-2016

Garcia, R. R., López-Puertas, M., Funke, B., Marsh, D. R., Kinnison, D. E., Smith, A. K., & González-Galindo, F. (2014). On the distribution of CO_2 and CO in the mesosphere and lower thermosphere. *Journal of Geophysical Research: Atmospheres*, *119*(9), 5700–5718. https://doi.org/10.1002/2013JD021208

Geller, M. A., Alexander, M. J., Love, P. T., Bacmeister, J., Ern, M., Hertzog, A., & Zhou, T. (2013). A comparison between gravity wave momentum fluxes in observations and climate models. *Journal of Climate*, *26*(17), 6383–6405. https://doi.org/10.1175/JCLI-D-12-00545.1

Gérard, J.-C., Roble, R. G., Rusch, D. W., & Stewart, A. I. (1984). The global distribution of thermospheric odd nitrogen for solstice conditions during solar cycle minimum. *Journal of Geophysical Research: Space*, *89*, 1725–1738. https://doi.org/10.1029/JA089iA03p01725

Gettelman, A., Hannay, C., Bacmeister, J. T., Neale, R. B., Pendergrass, A. G., Danabasoglu, G., & Mills, M. J. (2019). High climate sensitivity in the community Earth system model version 2 (cesm2). *Geophysical Research Letters*, *46*(14), 8329–8337. https://doi.org/10.1029/2019GL083978

Gordley, L. L., Hervig, M. E., Fish, C., Russell, J. M., Bailey, S., Cook, J., & Kemp, J. (2009). The solar occultation for ice experiment. *Journal of Atmospheric and Solar-Terrestrial Physics*, *71*(3–4), 300–315. https://doi.org/10.1016/j.jastp.2008.07.012

Hendrickx, K., Megner, L., Marsh, D. R., & Smith-Johnsen, C. (2018). Production and transport mechanisms of no in the polar upper mesosphere and lower thermosphere in observations and models. *Atmospheric Chemistry and Physics*, *18*(12), 9075–9089. https://doi.org/10.5194/acp-18-9075-2018

Hurrell, J. W., Holland, M. M., Gent, P. R., Ghan, S., Kay, J. E., Kushner, P. J., & Marshall, S. (2013). The community Earth system model: A framework for collaborative research. *Bulletin of the American Meteorological Society*, *94*1339–1360. https://doi.org/10.1175/BAMS-D-12-00121.1

IPCC. (2013). *Climate change 2013: The physical science basis contribution of working group 1 to the fifth assesment report of the intergovernmental panel on climate change*. Cambridge University Press.

Jackman, C. H., Marsh, D. R., Vitt, F. M., Garcia, R. R., Fleming, E. L., Labow, G. J., & Stiller, G. P. (2008). Short- and medium-term atmospheric constituent effects of very large solar proton events. *Atmosheric Chemistry and Physics*, *8*(3), 765–785. https://doi.org/10.5194/acp-8-765-2008

van de Kamp, M., Seppälä, A., Clilverd, M. A., Rodger, C. J., Verronen, P. T., & Whittaker, I. C. (2016). A model providing long-term data sets of energetic electron precipitation during geomagnetic storms. *Journal of Geophysical Research Atmosphere*, *121*(20), 12520–12540. https://doi.org/10.1002/2015JD024212

Kunz, A., Pan, L. L., Konopka, P., Kinnison, D. E., & Tilmes, S. (2011). Chemical and dynamical discontinuity at the extratropical tropopause based on start08 and waccm analyses. *Journal of Geophysical Research: Atmospheres*, *116*, D24302. https://doi.org/10.1029/2011JD016686

Maliniemi, V., Asikainen, T., Salminen, A., & Mursula, K. (2019). Assessing north atlantic winter climate response to geomagnetic activity and solar irradiance variability. *Quarterly Journal of the Royal Meteorological Society*, *145*(725), 3780–3789. https://doi.org/10.1002/qj.3657

Marsh, D. R., Solomon, S. C., & Reynolds, A. E. (2004). Empirical model of nitric oxide in the lower thermosphere. *Journal of Geophysical Research: Space Physics*, *109*(A7), A03701. https://doi.org/10.1029/2003JA010199

Matthes, K., Funke, B., Anderson, M., Barnard, L., Beer, J., Charbonneau, P., & Versick, S. (2017). Solar forcing for cmip6 (v3.1). *Geoscientific Model Development*, *10*, 1–82. https://doi.org/10.5194/gmd-10-2247-2017

McFarlane, N. A. (1987). The effect of orographically excited gravity wave drag on the general circulation of the lower stratosphere and troposphere. *Journal of the Atmospheric Sciences*, *44*, 1775–1800. https://doi.org/10.1175/1520-0469(1987)044<1775:teooeg>2.0.co;2

Meraner, K., & Schmidt, H. (2016). Transport of nitrogen oxides through the winter mesopause in hammonia. *Journal of Geophysical Research: Atmospheres*, *121*(6), 2556–2570. https://doi.org/10.1002/2015JD024136

Meraner, K., Schmidt, H., Manzini, E., Funke, B., & Gardini, A. (2016). Sensitivity of simulated mesospheric transport of nitrogen oxides to parameterized gravity waves. *Journal of Geophysical Research: Atmospheres*, *121*(20), 12045–12061. https://doi.org/10.1002/2016JD025012

Nesse Tyssøy, H., Haderlein, A., Sandanger, M. I., & Stadsnes, J. (2019). Intercomparison of the poes/meped loss cone electron fluxes with the cmip6 parametrization. *J. Geophys. Res. Space.*, *124*. https://doi.org/10.1029/2018JA025745

Nicolet, M. (1975). On the production of nitric oxide by cosmic rays in the mesosphere and stratosphere. *Planetary and Space Science*, *23*(4), 637–649. https://doi.org/10.1016/0032-0633(75)90104-X

Randall, C. E., Harvey, V. L., Singleton, C. S., Bailey, S. M., Bernath, P. F., Co-drescu, M. V., & Russell, J. M., III. (2007). Energetic particle precipitation effects on the southern hemisphere stratosphere in 1992-2005. *Journal of Geophysical Research: Atmospheres*, *112*. https://doi.org/10.1029/2006JD007696

Randall, C. E., Harvey, V. L., Singleton, C. S., Bernath, P. F., Boone, C. D., & Kozyra, J. U. (2006). Enhanced nox in 2006 linked to strong upper stratospheric arctic vortex. *Geophysical Research Letters*, *33*. https://doi.org/10.1029/2006GL027160

Remsberg, E. E., Marshall, B. T., Garcia-Comas, M., Krueger, D., Lingenfelser, G. S., Martin-Torres, J., & Thompson, R. E. (2008). Assessment of the quality of the version 1.07 temperature-versus-pressure profiles of the middle atmosphere from timed/saber. *Journal of Geophysical Research: Atmospheres*, *113*(D17). https://doi.org/10.1029/2008JD010013

Richter, J. H., Sassi, F., & Garcia, R. R. (2010). Toward a physically based gravity wave source parameterization in a general circulation model. *Journal of the Atmospheric Sciences*, *67*. https://doi.org/10.1175/2009JAS3112.1

Rienecker, M. M., Suarez, M. J., Gelaro, R., Todling, R., Bacmeister, J., Liu, E., & Woollen, J. (2011). Merra: Nasa's modern-era retrospective analysis for research and applications. *Journal of Climate*, *24*. https://doi.org/10.1175/JCLI-D-11-00015.1

Roble, R., & Ridley, E. (1987). An Auroral Model for the Ncar Thermospheric General Circulation Model (TGCM). *Annales Geophysicae Series A-Upper Atmoshphere And Space Sciences*, 5, 369–382.

Russell, J., Bailey, S., Gordley, L., Rusch, D., Horányi, M., Hervig, M., & Merkel, A. (2009). The aeronomy of ice in the mesosphere (aim) mission: Overview and early science results. *Journal of Atmospheric and Solar-Terrestrial Physics*, *71*, 289–299. https://doi.org/10.1016/j.jastp.2008.08.011

Russell, J. M. I., Mlynczak, M. G., Gordley, L. L., Tansock, J., & Esplin, R. (1999). *An overview of the saber experiment and preliminary calibration results*. Space Dynamics Lab Publications 3756. https://doi.org/10.1117/12.366382

Saetre, C., Stadsnes, J., Nesse, H., Aksnes, A., Petrinec, S. M., Barth, C. A., & Oestgaard, N. (2004). Energetic electron precipitation and the no abundance in the upper atmosphere: A direct comparison during a geomagnetic storm. *Journal of Geophysical Research: Space Physics*, *109*(A9). https://doi.org/10.1029/2004JA010485

Seppälä, A., Matthes, K., Randall, C. E., & Mironova, I. A. (2014). What is the solar influence on climate? Overview of activities during cawses-ii. *Progress in Earth and Planetary Science*, *1*. https://doi.org/10.1186/s40645-014-0024-3

Smith, A. K. (2012). Global dynamics of the mlt. *Surveys in Geophysics*, *33*, 1177–1230. https://doi.org/10.1007/s10712-012-9196-9

Smith, A. K., Garcia, R. R., Marsh, D. R., & Richter, J. H. (2011). Waccm simulations of the mean circulation and trace species transport in the winter mesosphere. *J. Geophys. Res. Atmos.*, *116*. https://doi.org/10.1029/2011JD016083

Smith-Johnsen, C., Marsh, D. R., Orsolini, Y., Nesse Tyssøy, H., Hendrickx, K., Sandanger, M. I., & Stordal, F. (2018). Nitric oxide response to the april 2010 electron precipitation event: Using waccm and waccm-d with and without medium-energy electrons. *Journal of Geophysical Research Space*, *123*(6), 5232–5245. https://doi.org/10.1029/2018JA025418

Swider, W., Keneshea, T., & Foley, C. (1978). An spe-disturbed d-region model. *Planetary and Space Science*, *26*(9), 883–892. https://doi.org/10.1016/0032-0633(78)90111-3

Tyssøy, H. N., Sinnhuber, M., Asikainen, T., Bender, S., Funke, B., Hendrickx, K., et al. (2021). Heppa III intercomparison experiment on electron precipitation impacts, part I: Estimated ionization rates during a geomagnetic active period in april 2010. *Journal of Geophysical Research - Space Physics*, *123*(6), e2021JA02198.

Verronen, P. T., Andersson, M. E., Marsh, D. R., Kovács, T., & Plane, J. M. C. (2016). Waccm-d—Whole atmosphere community climate model with d-region ion chemistry. *Journal of Advances in Modeling Earth Systems*, *8*(2), 954–975. https://doi.org/10.1002/2015MS000592

Verronen, P. T., & Lehmann, R. (2013). Analysis and parameterisation of ionic reactions affecting middle atmospheric ho_x and no_y during solar proton events. *Annales Geophysicae*, *31*(5), 909–956. https://doi.org/10.5194/angeo-31-909-2013

Weeks, L. H., Cuikay, R. S., & Corbin, J. R. (1972). Ozone measurements in the mesosphere during the solar proton event of 2 november 1969. *Journal of the Atmospheric Sciences*, *29*(6), 1138–1142. https://doi.org/10.1175/1520-0469(1972)029<1138:omitmd>2.0.co;2